Basrah Journal for Engineering Sciences, Vol. 20, No. 2, (2020), 48-59

Basrah Journal for Engineering Sciences

Journal homepage: www.bjes.edu.iq
ISSN (Online): 23118385, ISSN (Print): 18146120

OPEN ACCESS

Studying the Effect of Perforation Parameters on Vertical Well Performance

Haider Sami Mohammed [1,*], Emad Abdullah Khazal [2], Hussein Sadeq Sultan [3]

[1,2,3]*Department of Mechanical Engineering, College of Engineering, University of Basrah, Basrah, Iraq*
E-mail address: Eng.haider.sami@gmail.com , emad.khazal@uobasrah.edu.iq , hussein.sultan@uobasrah.edu.iq
Received: 4 November 2019; Accepted: 5 January 2020; Published: 2 March 2020

Abstract

This paper presents a pressure drop analysis in perforated vertical wellbores for different perforation parameters. The effect of the density of the perforations (number of perforation), the phase angle of the perforations, the diameter of the perforation and the flow rate of the crude oil from the perforations on the pressure drop and the productivity index of the perforated vertical wellbores were studied. The analysis of the vertical wellbore was performed numerically using ANSYS FLUENT 15.0 software. Three dimensional, steady-states, turbulent and incompressible fluid flow is assumed during the numerical solution of the governing equations. The results of this study show that, increased perforation density of the perforated vertical wellbore caused an increase in pressure drop, and also, decreased productivity index due to increasing the friction losses. Friction pressure drop has a significant effect on crude oil flow into the wellbore. When the main velocity is 1.5 m/s and the inlet velocity from the perforations is 2 m/s, the friction pressure drop is about 66 % and the acceleration pressure is approximately 34 % of the total pressure drop.

Keywords: Vertical wellbore, Perforation, Pressure drop, Productivity index, Inflow.

1. Introduction

In the field wellbore completion improvement, fluid flow in the wellbore and reservoir is concerned with the field researchers. The researchers are interested in single-phase and multi-phase flow to obtain information to the reservoir and the index of oil and gas production.

Oil and gas production wells prepared for production by general steps which are; firstly after drilling the production casing is perforated after the cementing. The perforation permits the fluid to flow into the wellbore. Perforating guns are used to create the perforation. The aim of perforating is to penetrate the casing, cement and extend into the virgin reservoir to provide a flow path for reservoir fluids to flow into the wellbore. Perforating design optimizes the gun configuration and wellbore conditions to achieve maximum productivity. Numerous studies have been performed on perforation parameters and the efficiency of flow. Karakas and Tariq [1] they studied the productivity of wellbore for various parameters of reservoir and perforations for two cases, 2D and 3D finite element for the inflow of perforations. They presented a semi-analytical solution for the wellbore productivity ratio. Their results showed that the crushed zone around perforations essentially increases the vertical resistance to flow and the productivity ratio increases with increasing perforation length. Ansah et al. [2] developed a model for wellbore inflow that can be used for studying the effect perforation shot density, entrance casing hole, perforation phase angle and the damage around the perforation on the wellbore productivity. A numerical solution for 3D flow was performed using ANSYS 5.7 based on the finite element method. Their results showed that, the performance of wellbore production affected by the shape of perforations. The length of the conical perforation has a significant influence on flow performance. Also, the pipe diameter has an important effect on the productivity ratio. Yildiz [3] developed a semi-analytical 3D model for a perforated vertical wellbore. The model can be used to predict the relationship for the inflow performance of the wells. The predictions of the model have been compared with experimental data for verification. The results showed that the permeability of the zone around the perforation has an important effect on the productivity of the well. Hagoort [4] in this study the productivity of perforated wells have been predicted by using an analytical model. In this model, the solution for single-phase, and Darcy flow for single perforation in the porous medium. Was obtained the model gives an equation for the perforation skin as a function of the important perforation parameters. The results show that, the productivity ratio increase with increasing perforation length, while the perforation diameter has a slight effect on productivity ratio. Fayal and Lakhdar [5] studied the effect of friction and acceleration losses in perforated horizontal wellbore on a total pressure drop. The conditions of the flow are steady-state, Newtonian, incompressible flow and single-phase flow. The flow model was solved by using CFD simulation FLUENT program. The results show that acceleration pressure drops about 30 % of the total pressure drop. Xu et al. [6] studied how perforations distribution effect on the productivity of a vertical well. A programming algorithm is applied to vertical well optimization models established under finite and infinite conductivity, respectively. HTHP (high-temperature high pressure) gas well was studied to demonstrate how the model through optimization of the perforation position and there was a

reasonable perforation density distribution. Experimental results showed that the pressure drop in HTHP perforated vertical well consisted of gravitational is about 80 %, friction is more than 15 % and acceleration is nearly 5 %. The optimal perforation distribution and production along the perforated vertical well is plotted with an infinite conductivity well and a finite conductivity well considering both a coning effect and a no coning effect. Abdulwahid et al. [7] studied the effect of flow behavior on pressure drop in a horizontal wellbore, for two cases 60 and 150 of perforations density, which equivalent to 6 and 12 SPF respectively. By using ANSYS CFX modeling tool with different Reynolds number and different influx flow rate to observe the flow through a perforated pipe. Their results showed that, increased flow rate and the density of the perforations lead to increased total pressure drop, while the friction pressure drop increases with increasing the perforation density. Elsharafi et al. [8] studied the effect of perforation parameters on vertical wellbore productivity. This study was concentrated on the effect of damaged skin factor, crushed zone skin factor and perforation skin factor. Also, the calculation method for the perforation depth and flow rate for different kinds of guns is used. They concluded that, increasing the depth of the hole causes an increase in fluid flow while the skin factor decreases. Also, the flow rate decrease with increasing the skin factor. Salim et al. [9] studied the effect of the shape and diameter of the perforations on the total pressure drop of a perforated vertical wellbore. He assumed that single phase, turbulent flow and phase angle 180 for two perforations. Also, using as water a working fluid and by using ANSYS CFX for numerical simulation. The results showed that, increase the diameter and flow velocity of the perforations causing an increase in pressure drop. The cylindrical shape of the perforated is more pressure drop than the conical shape of the same parameters and the length of the perforation has a very small effect on the pressure drop and can be neglected.

This study aims to have a better understanding on how the productivity of vertical wellbore affected by pressure drop, this paper presented CFD model in a perforated vertical wellbore to study the influence of wellbore diameter, diameter, and length of perforation, perforation phase angle and shot density on each of pressure drop, friction factor, wall shear stress, and velocity distribution.

2. Numerical Simulations

In the present time, there is the ability to use modeling software which can be used to simulate the fluid flow. In the present study numerical solution for 3D study flow using FVM are performed. The simulation was performed using ANSYS FLUENT 15.0 software [10].

3. Description of the Cases

In this study, the numerical simulation for vertical wellbore with the following specification: for 1m length (L) and the internal diameter (D) is 0.154 m (6 in), the dimensions of all perforation were 35 mm length (lp) with a diameter (d) of 10 mm (13/32 in), the distance between two consecutive perforations (h) is constant and equal to 0.05 m, as shown in Fig. 1. The effect of the following parameters was studied: firstly, the effect of the perforation phase angle on pressure drop was studied. For phase angles considered which are (360°,180°, 90° and 60°), as shown in Fig. 2, with the density of perforations (number of perforation) on total pressure, friction factor, shear stress, and productivity index are studied. Secondly, the effect of the helical distribution of the perforations at 60° phase angle, with the number of perforation on the total pressure, acceleration pressure, and friction pressure are studied.

The numerical simulations results were compared with the theoretical calculations.

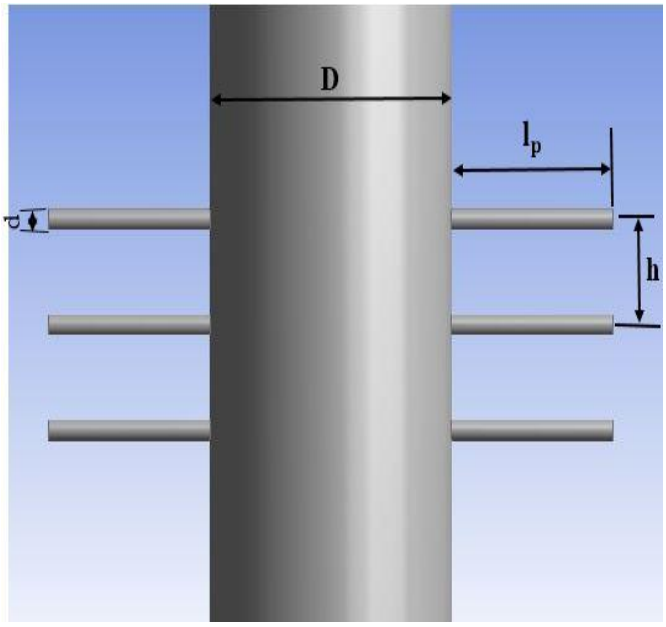

Fig. 1 Six perforations with 180° phase angle.

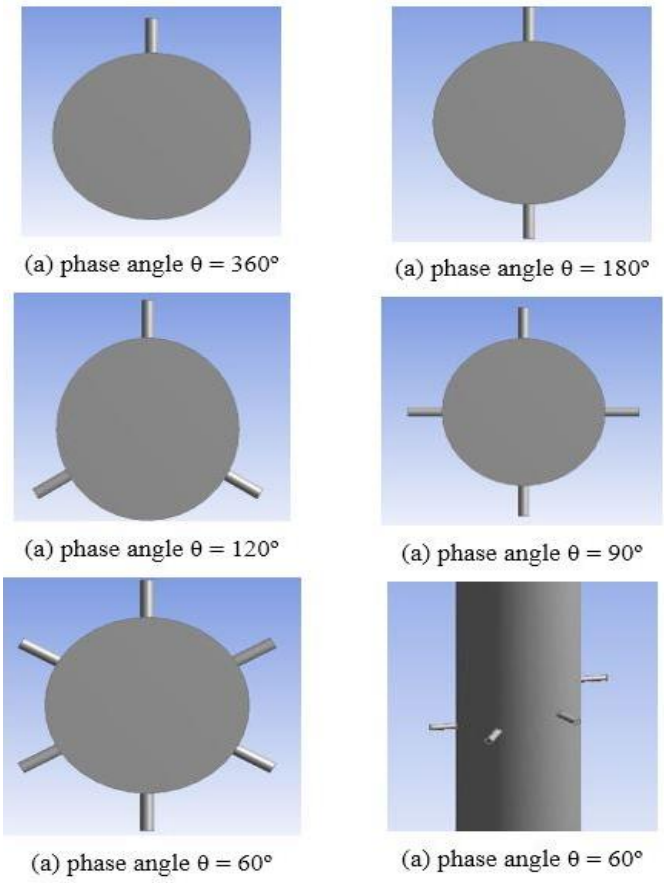

Fig. 2 Phase angle of the perforated vertical wellbore.

4. Assumptions and simulation Parameters

The following assumptions are applied during the simulation. Three-dimensional steady flow for single-phase and Newtonian fluid flow. The gravity effect is neglected and the perforation is perpendicular to the direction of the wellbore fluid flow. The working fluid is crude oil with the following properties; density 842 kg/m^3, viscosity 0.006 (kg/m.s) and the temperature 15 °C.

5. Boundary Conditions

The governing equations system in CFD can be solved only if there are boundary conditions to fulfill a solution. Therefore, we need to provide boundary conditions to a CFD solver. There are various forms of boundary inputs that convert a real situation to its CFD model counterpart. ANSYS FLUENT allows several methods for the definition of a fluid boundary. In this study, use the boundary conditions given below:

1. The velocity inlet of the wellbore (u_1) is 1.5 m/s, while the velocity inlet from perforations (u_2) is 2 m/s.
2. The outlet boundary condition is pressure (P_o) equal zero.
3. The wall boundary condition is the roughness of the wall is considered an equal to 0.01 mm, as shown in Fig. 3.

Medium Turbulence Intensity = 5 % (a viscosity ratio μ/μ_t equal to 10) for both inlets.

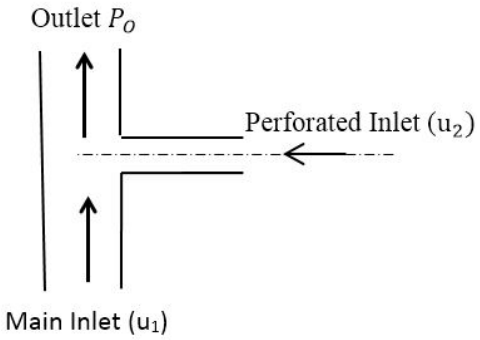

Fig. 3 Flow from Perforation and wellbore.

6. Governing Equations

Fluid flow in perforated vertical wellbore undergoes a considerable measure of physical changes such as pressure. The change of the pressure is due to friction losses in vertical pipe and perforations, mixing, acceleration and gravity, velocity change caused by varying flow regimes and density, and kinetic energy change. In order to properly describe these physical changes, we need to solve the two governing equations of fluid flow (mass and momentum equations). The mathematical statements representation of the conservation of physical laws is given below [11, 12 and 13].

6.1. Conservation of Mass

Based on the mass balance for the fluid element, we can derive the conservation of mass equation which is given as:

$$\rho \frac{\partial}{\partial x_i}(u_i) = 0 \tag{1}$$

Where,
$u_i = u\,i + v\,j + w\,k$ is the velocity vector in the Cartesian coordinate.

For turbulent flow, breaking the instantaneous velocity into mean and fluctuating components is defined as:

$$u_i = \overline{u_\iota} + u_i' \tag{2}$$

Where,
$\overline{u_\iota}$: The mean velocity vector.
u_i' : The fluctuating velocity vector.
Substituting Eq. (2) into Eq. (1) and then integrating by time-averaged, or Reynolds-averaged, with taking into consideration the average of fluctuating equal to zero, this yields the Reynolds-averaged continuity equation for incompressible flow.

$$\frac{\partial \overline{u_\iota}}{\partial x_i} = \frac{\partial \bar{u}}{\partial x} + \frac{\partial \bar{v}}{\partial y} + \frac{\partial \bar{w}}{\partial z} = 0 \tag{3}$$

6.2. Conservation of Momentum

The conservation of momentum equation in Cartesian coordinates is given as:

$$\frac{\partial}{\partial t}(\rho u_i) + u_j \frac{\partial(\rho u_i)}{\partial x_j} = -\frac{\partial P}{\partial x_i} + \frac{\partial}{\partial x_j}(\tau_{ji}) + F_i \tag{4}$$

Where,
$u_j = u\,i + v\,j + w\,k$ is the velocity vector in the Cartesian coordinate.

The viscous stress tensor can be rewritten in terms of the strain rate tensor by.

$$\tau_{ji} = \mu\left(\frac{\partial u_j}{\partial x_i} + \frac{\partial u_i}{\partial x_j}\right) = 2\mu S_{ji} \tag{5}$$

Where,
τ_{ji} : The viscous stress tensor.
S_{ji} : The strain rate tensor (rates of deformation of a fluid element).
Substitute Eq. (5) into Eq. (4) yields,

$$\rho \frac{\partial}{\partial x_j}(u_i u_j) = -\frac{\partial P}{\partial x_i} + \frac{\partial}{\partial x_j}(2\mu S_{ji}) + F_i \tag{6}$$

In turbulent flow, the instantaneous quantities can be broken up into mean and fluctuating components.

$$u_i = \overline{u_\iota} + u_i'.\;\; u_j = \overline{u_j} + u_j'.\;\; P = \bar{P} + P'$$

$$S_{ji} = \bar{S}_{ji} + S_{ji}' \tag{7}$$

Substituting Eq. (7) into Eq. (6) and taking the time-averaged, yields the momentum equation for incompressible flow. Typically called Reynolds-averaged Navier-Stokes.

$$\rho \bar{u}_j \frac{\partial}{\partial x_j}(\overline{u_i}) = -\frac{\partial \bar{P}}{\partial x_i} + \frac{\partial}{\partial x_j}\left(2\mu \bar{S}_{ji} - \rho \overline{u_\iota' u_j'}\right) + F_i \tag{8}$$

The minus sign of the average static pressure $\bar{P}$ due to compressive normal stress, because the usual sign agreement takes tensile stress to be the positive normal stress. The last term in Eq. (8) represents a body forces acting through the

fluid of the element which is gravity force, centrifugal force, Coriolis force, and electromagnetic force.
Where,
$\rho\overline{u_i'u_j'}$: The Reynolds stresses or turbulent stresses tensor.

In order to compute the Reynolds stresses we use the familiar Boussinesq relationship:

$$\rho\overline{u_i'u_j'} = \frac{2}{3}k\delta_{ij} - \mu_t\left(\frac{\partial\bar{u}_j}{\partial x_i} + \frac{\partial\bar{u}_i}{\partial x_j}\right) \quad (9)$$

Where,
δ_{ij} : The Kronecker delta, $\delta_{ij} = 1$ if $i = j$ and $\delta_{ij} = 0$ if $i \neq j$.
μ_t : The eddy viscosity or turbulent viscosity.
k : The kinetic energy of turbulent fluctuations.

7. Turbulence models (Stander k-ϵ model)

The standard k-∈ model belongs to the general group of two-equation models, which tackle two separate transport equations and they are the most widely used in industrial applications because of it provides economy, robustness and reasonable accuracy. The standard k-∈ model uses the following transport equations for k,

$$\rho u_j\frac{\partial \mathrm{k}}{\partial x_j} = \frac{\partial \mathrm{k}}{\partial x_j}\left((\mu + \frac{\mu_t}{\sigma_k})\frac{\partial \mathrm{k}}{\partial x_j}\right) + 2\mu_t S_{ij}.S_{ij} - \rho\epsilon \quad (10)$$

and ϵ;

$$\rho u_j\frac{\partial \epsilon}{\partial x_j} = \frac{\partial \epsilon}{\partial x_j}\left((\mu + \frac{\mu_t}{\sigma_\epsilon})\frac{\partial \epsilon}{\partial x_j}\right) + C_{1\epsilon}\frac{\epsilon}{k}\mu_t S_{ij}.S_{ij} - C_{2\epsilon}\rho\frac{\epsilon^2}{\mathrm{k}} \quad (11)$$

Where, σ_k and σ_ϵ are the Prandtl numbers connecting the diffusivities of k and ϵ to the eddy viscosity μ_t, the strain rate tensor can be rewritten in terms of velocity by.

$$S_{ji} = \frac{1}{2}\left(\frac{\partial u_j}{\partial x_i} + \frac{\partial u_i}{\partial x_j}\right) \quad (12)$$

It is noticeable that the transport equations include five adjustable constants $\sigma_k, \sigma_\epsilon, C_\mu, C_{1\epsilon}$ and $C_{2\epsilon}$. The values for these constants have been obtained by comprehensive data fitting to the standard $\mathrm{k}-\epsilon$ model for a wide range of turbulent flows. These values are following [14]:
$\sigma_k = 1.00,\ \sigma_\epsilon = 1.30,\ C_\mu = 0.09,\ C_{1\epsilon} = 1.44$ and $C_{2\epsilon} = 1.92$.

8. Theoretical Model

The total pressure drop in a perforated vertical wellbore can be divided into four sources, as given by the following relationship:

$$\Delta P_T = \Delta P_f + \Delta P_g + \Delta P_{mix} + \Delta P_{acc.} \quad (13)$$

8.1. Friction Pressure Drop

Friction is significant affects the pressure drop. Friction pressure drop is caused by the resistance to the fluid movement. Many researchers have focused on studying the effect of friction and the most important researchers are [15, 16, 17, 18 and 19]. The equation that describes a friction pressure drop in perpendicular wells is a Darcy-Weisbach equation.

$$\Delta P_f = f_t\frac{L}{D}\frac{\rho u^2}{2} \quad (14)$$

The Eq. (14) is used to calculate the friction pressure drop theoretically. Also, the friction pressure drop can be obtained from FLUENT directly as a pressure difference between outlet and inlet.

8.2. Friction Factor (f_t)

The friction factor represents the fluid force affecting the walls; there is a set of equations that can calculate the friction factor, for both smooth walls and rough walls during turbulent flow. As in the following equation:

$$f_t = f_o + f_p \quad (15)$$

Friction factor for an unperforated pipe is given using Haaland equation [20], which is given below:

$$\frac{1}{\sqrt{f_o}} = -1.8\log\left(\frac{6.91}{\mathrm{Re}} + \left(\frac{\mathrm{e}}{3.7\ \mathrm{D}}\right)^{1.11}\right) \quad (16)$$

The Reynolds number can be calculated from the equation (17), where the Reynolds number represents the ratio between inertia forces to viscous force.

$$Re = \frac{\rho u D}{\mu} \quad (17)$$

The friction losses due to inflow from perforations are calculated using the Acheim equation [21], which is given by the following.

$$f_p = 4D\ \frac{q}{Q} + 2\frac{D}{n}(\frac{q}{Q})^2 \quad (18)$$

Where, q represents the flow rate from perforations, expressed which is by the equation below:

$$q = n\frac{\pi}{4}d^2u_2 \quad (19)$$

Also, can be using the Darcy equation to obtain the total friction factor numerically in terms of static pressure drop from FLUENT.

$$f_t = \Delta P_s\frac{D}{L}\frac{2}{\rho u^2} \quad (20)$$

8.3. Acceleration pressure drop

Pressure drop due to fluid flow acceleration caused by kinetic energy changes depends on the radial velocity of inflow fluid from perforation. The acceleration pressure drop is relatively more important in a small diameter than in a large diameter pipe. The acceleration pressure drop can be calculated theoretically and expressed as:

$$\Delta P_{acc.} = \rho \left[u_3^2 - (u_1^2 + u_2^2 \frac{A_p}{A_m} cos\, \alpha) \right] \quad (21)$$

The last term represented the effect of inflow angle when the perforation direction is exactly perpendicular on vertical wellbore this term equal to zero. The reduction of the inflow angle contributes to decreasing the acceleration pressure drop. For numerical calculation, all the velocities are obtained from FLUENT. The outlet velocity can be calculated theoretically from the conservation equation of mass for an incompressible fluid, as shown below:

$$u_3 = u_1 + u_2 \frac{A_p}{A_m} \quad (22)$$

The main inlet velocity and velocity inlet from perforation are specified in boundary conditions.

8.4. Mixing pressure drop

Mixing pressure drop is caused by the mixing of the main wellbore flow with the fluid flow of the perforations. Su and Gudmundsson [22] Developed an equation to calculate the magnitude of mixing pressure drop theoretically, when the flow rate ratio is larger than 0.0025 by the equation below:

$$\Delta P_{mix} = 760 \left(\frac{q}{Q} \right) \quad (23)$$

8.5. Productivity index (PI)

Productivity index for the vertical wellbore is given by the equation below:

$$PI = \frac{Q_3}{\Delta P_T} \quad (24)$$

Where, Q_3 is the amount of the lifting flow rate and ΔP_T is the pressure energy required for lifting.

9. Grid Independence Test

In order to ensure the grid independent solution, the first step of the numerical simulation is identifying the maximum mesh size, which is used to solve in ANSYS FLUENT 15.0 commercial software. Varying the maximum size of the mesh is applied to show the best mesh properties which can be used to simulation the cases in a present study. ICEM CFD 15.0 is used to generate the mesh with different maximum mesh size. The geometry of fluid flow is a vertical well 0.1524 m (6 in) diameter and length is 1 m with four perforations at center vertical distance and 90º perforation phase angle, the perforation diameter is 0.01 m (13/32 in) and the length is 0.0320 m from the surface of the well.

The grid independency of all the maximum mesh size based on the total pressure drop and average static pressure at the center point as shown in Fig. 4. Table 1 in appendix 1 explained the information about the grid independence test.

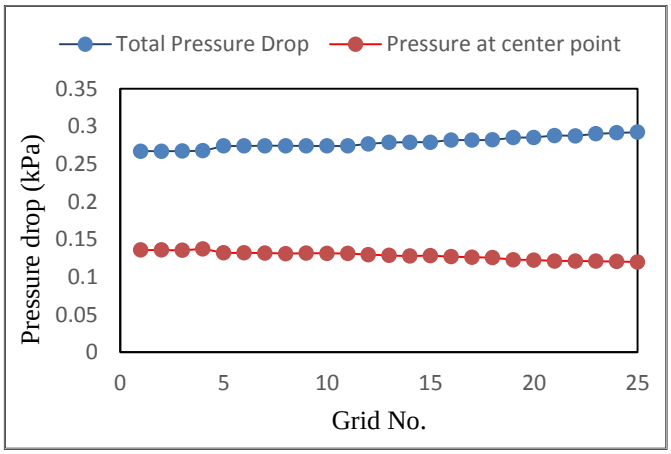

Fig. 4 Comparison of Pressure drop for Varying Mesh Size.

When the repeat of the maximum size mesh change, found the stability in the total pressure drop and static pressure between grid 5 to 15. The minimum percentage error of the predicted average static pressure lies between the previous and the next of the maximum mesh size of 0.00575 (Grid 14) with 308020 elements and nodes is 295294. Where was the percentage error between grid 14 and grid 15 for total pressure drop is less than (0.01 %) and (0.07 %) of static pressure at the center point.

10. Model Validation

In order to verify the accuracy of the numerical results of the current work. A comparison with the results of Salim et al. [23] is performed. They used CFD to simulate a perforated well. A three dimensional well with multi-perforation, as shown in Fig. 5. The length of the well is 1 m and the diameter is 0.2 m. The perforation length is 0.15 m; the diameter is 0.012 m and 180º phase angle.

The boundary conditions for this validation are as follows; the inlet velocity is 2.5 m/s, while the velocity from each perforation is 1 m/s and the static pressure at the well outlet is equal zero. The wall is smooth, no-slip boundary and neglects the effect of gravity.

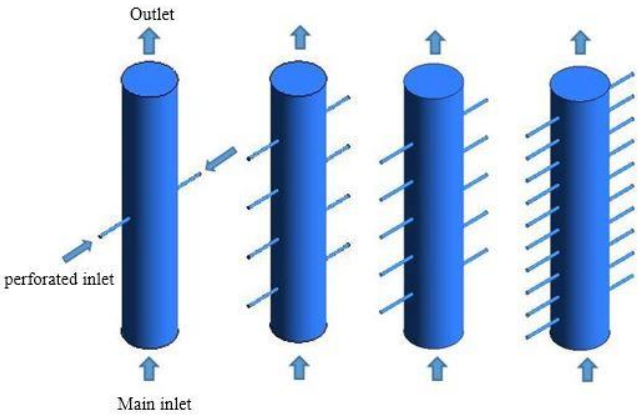

Fig. 5 Geometry of Perforated vertical wellbore with multi-perforation with 180º.

The ANSYS CFX 15.0 and FLUENT with Turbulence models (Stander k-ε model) are used to simulation, the steady-state, incompressible and 3D fluid flow. The results of this validation for the total pressure drop to all were cases very acceptable, as shown in Fig. 6. The maximum errors between Salim et al. and the current work using ANSYS CFX 15.0 is less than 3 %, while by using FLUENT the maximum error increase of about 6 %.

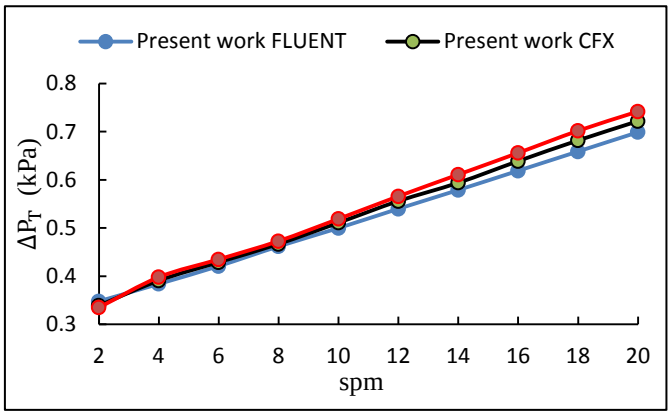

Fig. 6 Comparison of the total pressure drop with Salim et al.

11. Results and Discussion

11.1. Effect of shot density of perforations

Figure 7 illustrates the total pressure drop variation with the shot density for different perforation phase angle. The total pressure is affected significantly with increasing the density of the perforations. The increasing of perforation density leads to an increase in the amount of crude oil entering the vertical wellbore, which implies increasing the kinetic energy near the wall as shown in the contour of the kinetic energy as given in Fig. 8. Thus, the total pressure drop increases.

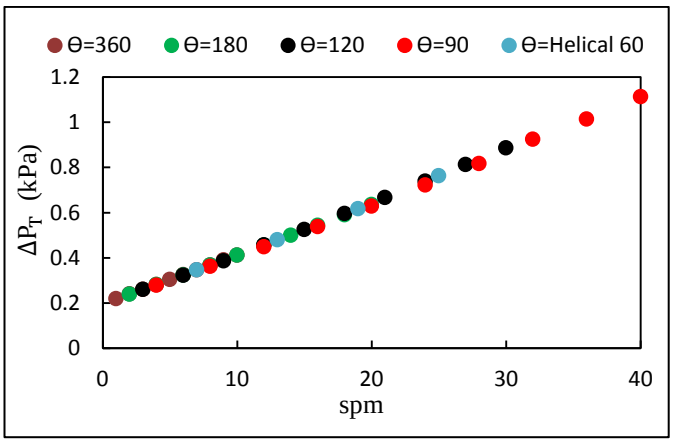

Fig. 7 Variation of total pressure drop with spm numerical results by FLUENT.

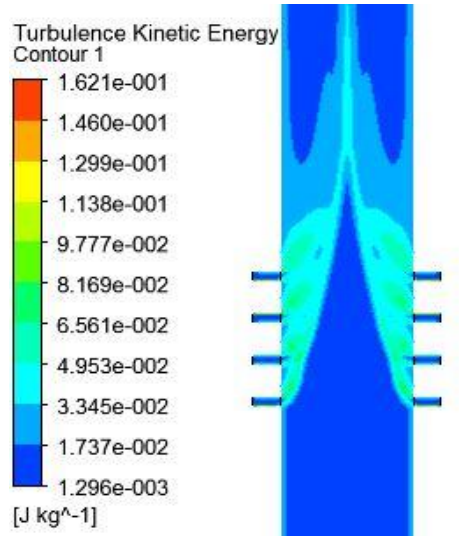

Fig. 8 Kinetic energy contour for 18 perforations with 180°.

Increase the density of the perforations causes an increase in the amount of crude oil entering the wellbore, this leads to an increase in the friction factor as shown in Fig. 9. Also, the friction factor increases due to the reduce velocity near the wall as shown in Fig. 10.

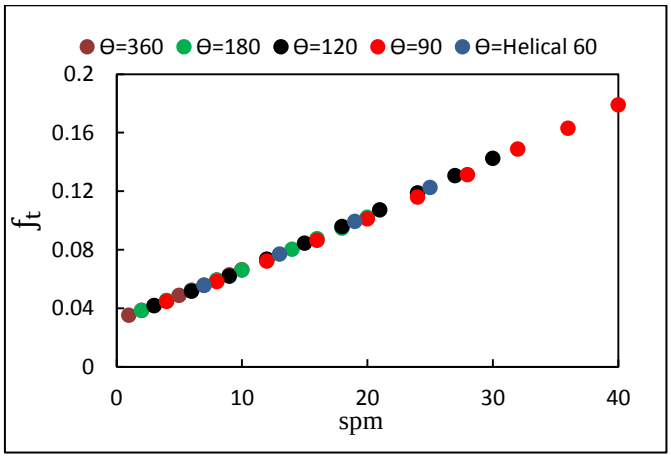

Fig. 9 Variation of friction factor with spm.

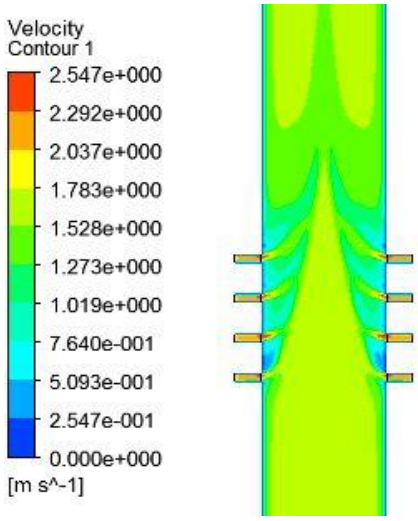

Fig. 10 Velocity contour for 8 perforations with 180° phase angle.

Figure 11 shows the variation of shear stress rate with the density of the perforations. The shear stress increases with the increase in the density of the perforations, due to an increase in the flow rate of crude oil, which leads to an increase in flow velocity.

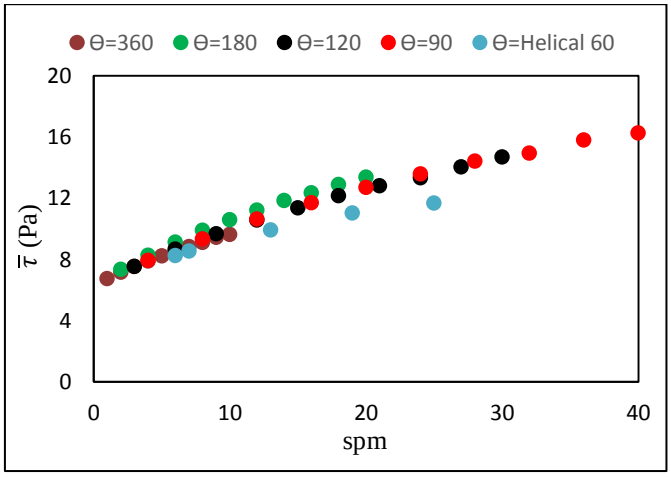

Fig. 11 Variation of average shear stress with spm.

The productivity index decreases with increasing the shot density, as a result of the increasing of the pressure drop with increasing the shot density more than the increasing inflow rate to the wellbore, as shown in Fig. 12. According to the equation (PI = Q/Pa). Figure 13 shows the contour of pressure distribution along 1 m vertical wellbore with 8 spm and 180° perforation phase angle, where the fluid flow rises up the pressure decrease due to pressure energy consumed.

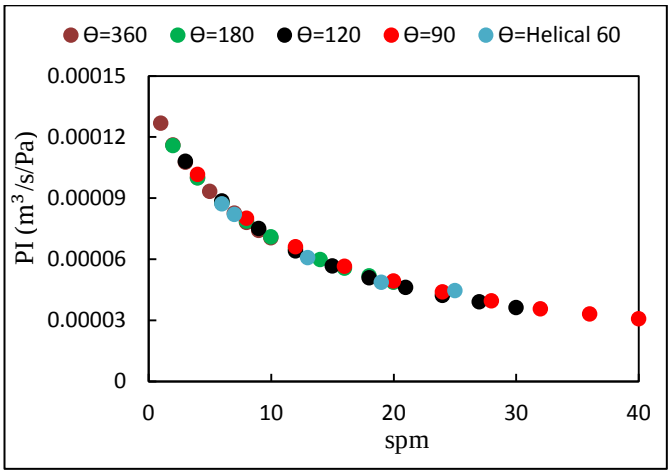

Figure 12 Variation of productivity index with spm.

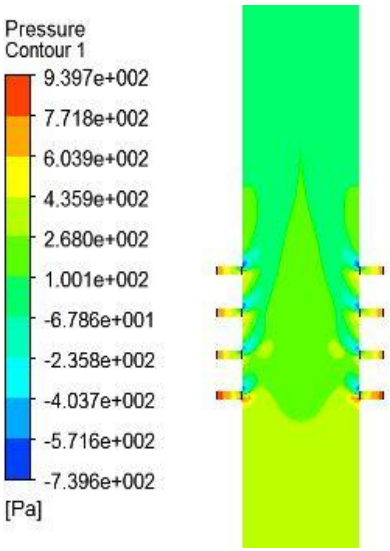

Fig. 13 Pressure contour for 8 perforations with 180° phase angle.

11.2. Effect of phase angles with a constant number of perforations (n = 6)

Figures 14, 15, 16, 17 and 18 show the effect of perforation phase angles on total pressure drop, friction factor, average wall shear, and productivity index respectively numerically and theoretically. From all the figures, it is clear that the impact of the perforation phase angle can be neglected. Because the fluid flow from the main pipe affected by the amount of inflow rate entrance from perforations, and not affected by phase angle location of perforations through a circumference of a vertical wellbore. The average error between numerical and theoretical results is about 11 %.

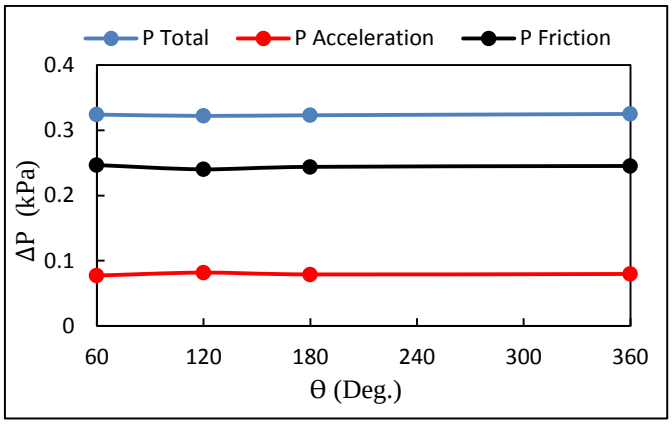

Fig. 14 Variation of total pressure drop with phase angle FLUENT.

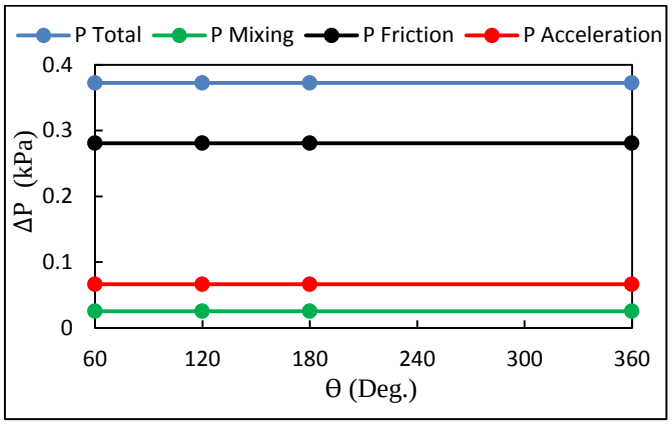

Fig. 15 Variation of total pressure drop with phase angle theoretical.

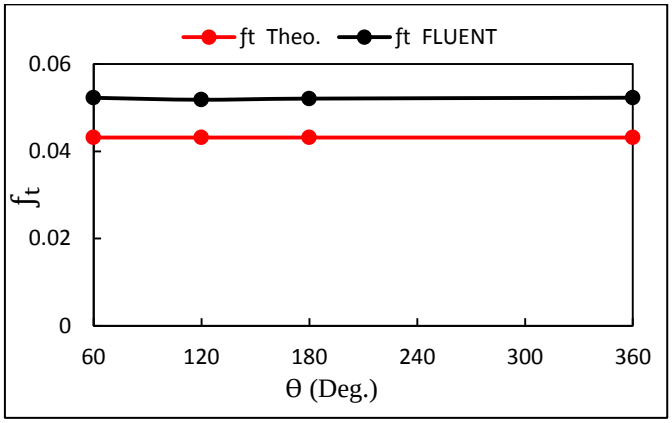

Fig. 16 Variation of friction factor with phase angle.

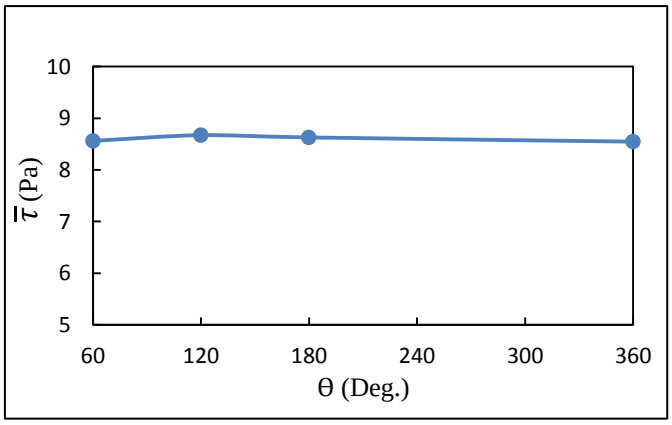

Fig. 17 Variation of average shear stress phase angle.

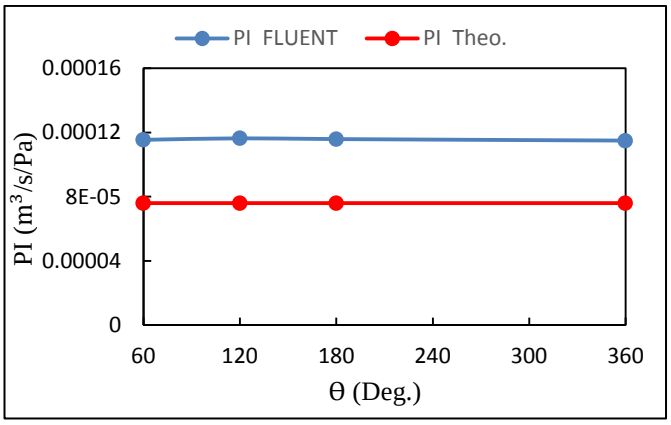

Fig. 18 Variation of productivity index phase angle.

11.3. Effect perforations shot density with constant phase angle (Helical 60°).

Figure 19 illustrates the variation of the total pressure drop components with perforations of the shot density, numerically using ANSYS FLUENT and theoretically. The components of the total pressure drop increase with increasing the density of the perforations.

When the main velocity (u_1) is 1.5 m/s and the entry velocity from the perforations (u_2) is 2 m/s. The numerical results were obtained, the friction pressure drop is about 66 % and the acceleration pressure drop is approximately 34 % of the total pressure drop. While the theoretical results obtained from the equations are as follows, the friction pressure is approximately 62 %, the acceleration pressure is 29 % and the mixing pressure drop is 7 % of the total pressure loss as shown in Fig. 20. The average error between numerical and theoretical results is about 6.5 % for total pressure losses. For numerical results, there is no ability to obtain a mixing pressure drop. Figure 21 illustrates the variation of the friction factor with the density of the perforations of the helical distribution at phase angle 60°, using numerical and theoretical calculations. The increase in the density of perforations causes an increase in friction pressure drop and this leads to an increase in the friction factor. The average error between theoretical and numerical results is about 11 %.

The increase of perforation density of the wellbore causes an increase in the velocity gradient in the radial direction, this leads to increasing the shear stress as shown in Fig. 22.

Effect of perforation density on productivity index is shown in Fig. 23, the productivity index decreases with increasing perforation density due to increased friction pressure drop as shown in Fig. 24.

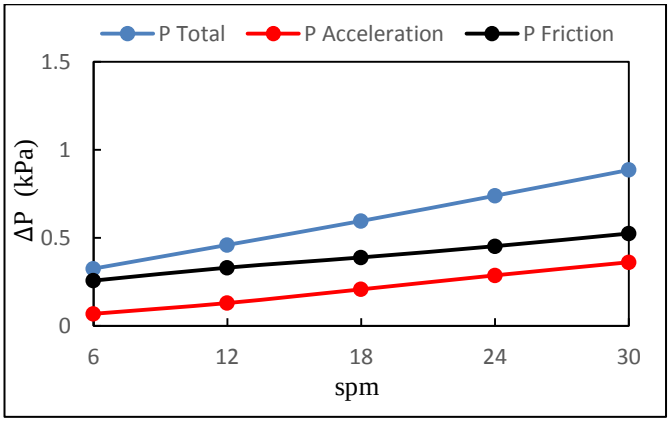

Fig. 19 Variation of component total pressure drop with spm FLUENT.

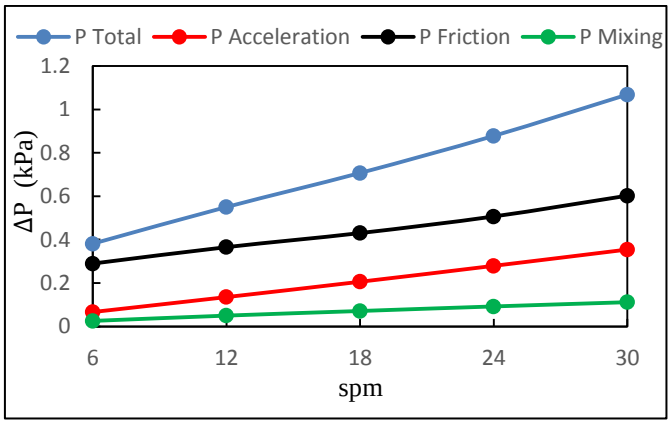

Fig. 20 Variation of components total pressure drop with spm theoretical.

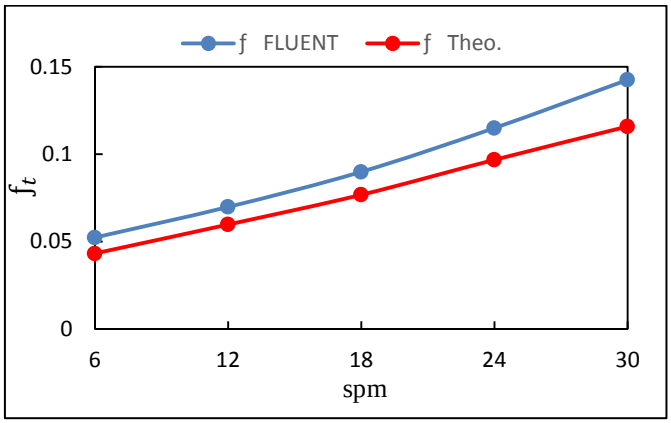

Fig. 21 Variation of friction factor with spm.

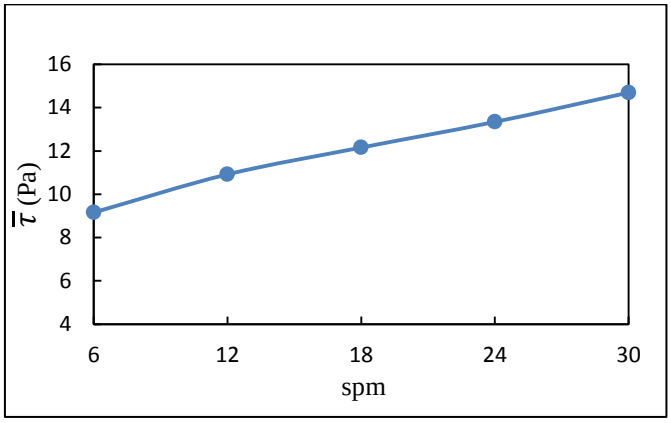

Fig. 22 Variation of average shear stress with spm.

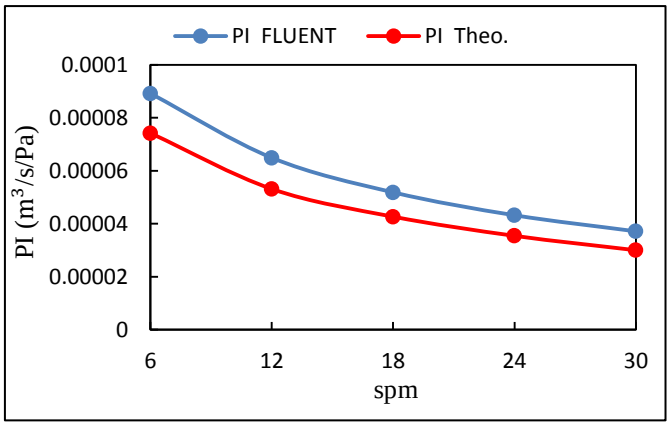

Fig. 23 Variation of productivity index with spm.

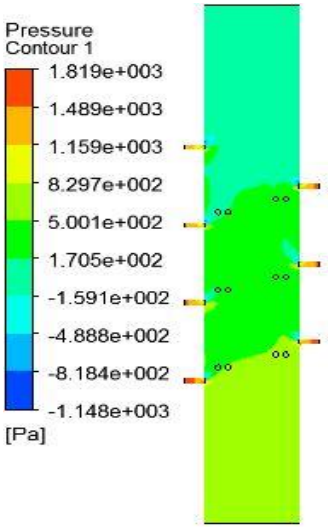

Fig. 24 Pressure contour for 18 perforations with helical 60°.

11.4. Effect of the diameter of the perforations for six perforations with (60° helical) phase angle

The pressure drop components as a function of perforation diameter for the constant density of perforation and phase angle with the helical distribution. Figures 25 and 26 explain the impact of the diameter of the perforations on pressure drop components, numerical by using FLUENT and theoretically by using equations. The results show that, the effect of the total pressure drop increasing to about 30 % when increasing the diameter from 8 mm to 14 mm, while the average error between the theoretical and numerical results did not exceed 9 %.

The friction factor variation with the diameter of the perforations is shown in Fig. 27. It is clear that the friction factor increases with increasing the diameter of the perforations due to increasing the crude oil inflow rate enter to the main wellbore. The results showed that, the effect of friction factor increasing about 27 % when increasing the diameter from 8 mm to 14 mm. The average error between the theoretical and numerical results does not exceed 7 %.

The average shear stress increases with increasing the diameter of the perforations as shown in Fig. 28, the effect of the average shear stress increasing about 19 % when increasing the diameter from 8 mm to 14 mm.

Figure 29 shows the decreasing of the productivity index with the increase of the diameter of the perforations, due to the increase of the total pressure drop. The productivity index lowered more than 32 % when increasing the diameter from 8 mm to 14 mm. The average error between numerical and theoretical results was less than 8 %.

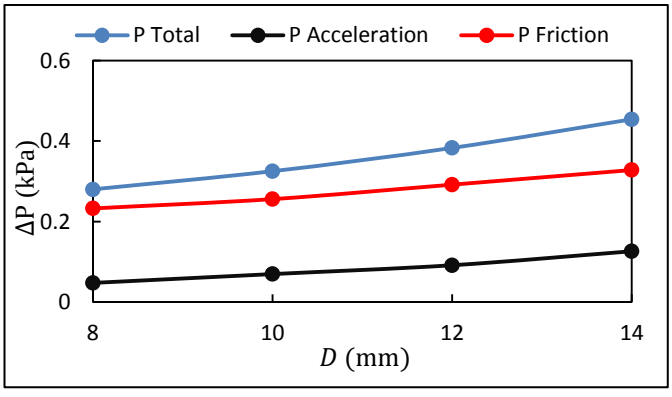

Fig. 25 Variation components total pressure drop with diameter FLUENT.

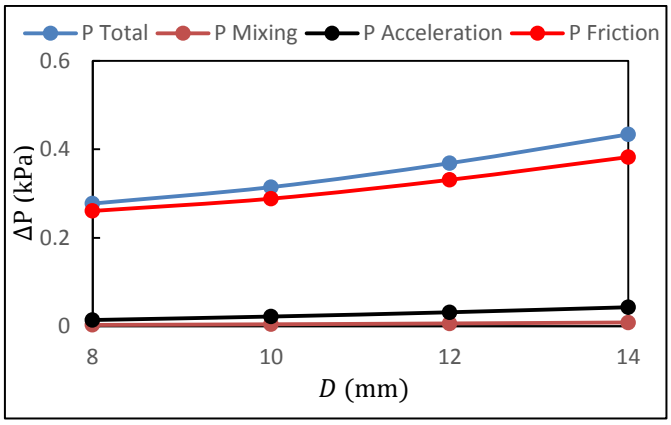

Fig. 26 Variation of components total pressure drop with diameter theoretical.

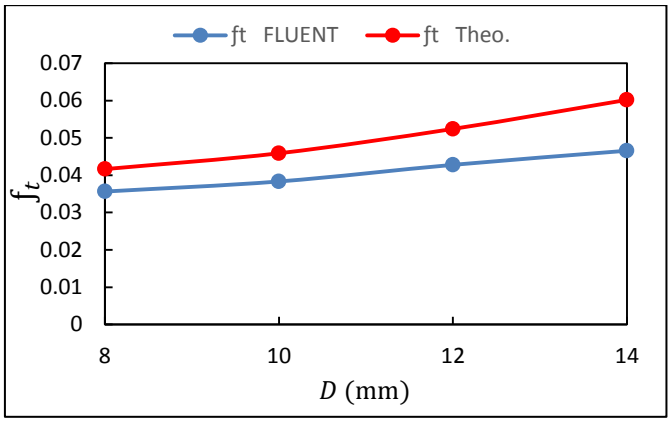

Fig. 27 Variation of friction factor with diameter.

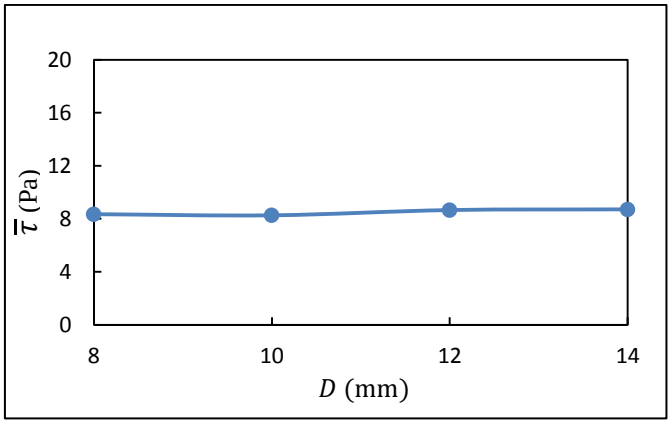

Fig. 28 Variation of average shear stress with diameter.

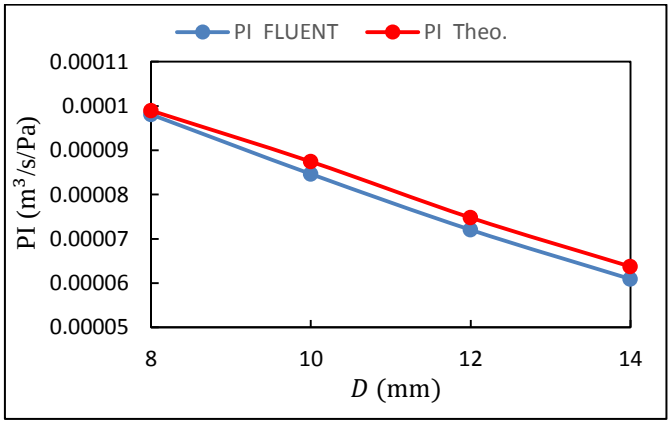

Fig. 29 Variation of productivity index with diameter.

11.5. Effect of the perforations velocity for six perforations with (60° helical distribution) phase angle

The velocity of the perforations is greatly influenced by the reservoir pressure. The velocity of the perforations increases with increasing the reservoir pressure. Figures 30 and 31 illustrate the effect of the perforations velocity on the pressure drop components numerically and theoretically respectively. The results showed that, the total pressure drop increases with the increasing velocity of perforations. The average error between numerical and theoretical results is less than 9 %.

The friction factor increases with the increasing of the perforation velocity as shown in Fig. 32, due to the increasing flow rate of crude oil into the wellbore. The difference between the numerical and theoretical results of the friction factor is less than 8 %. Also, the average shear stress increase with increasing the velocity of perforations as shown in Fig. 33. Figure 34 shows the productivity index decreases as the perforation velocity increases due to an increase in total pressure drop.

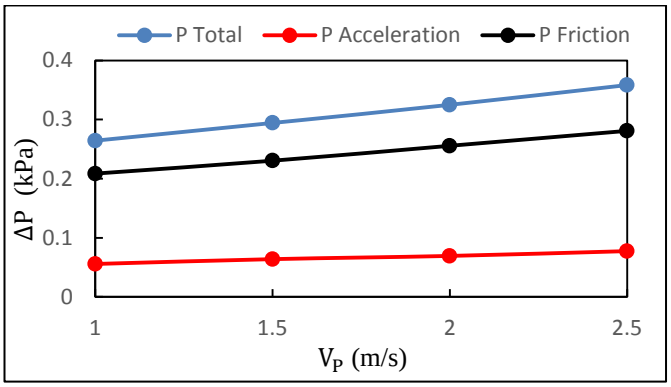

Fig. 30 Variation of components total pressure drop with perforation velocity FLUENT.

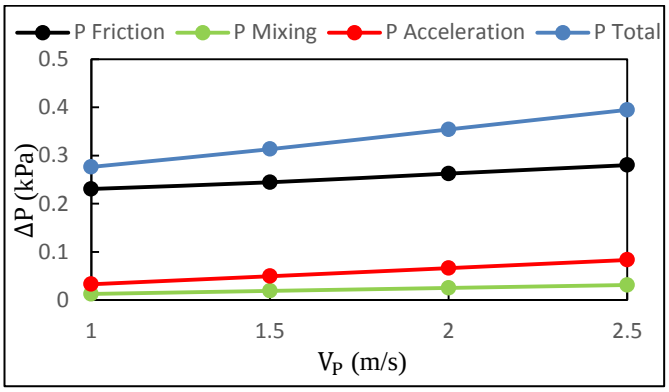

Fig. 31 Variation of components total pressure drop with perforation velocity theoretical.

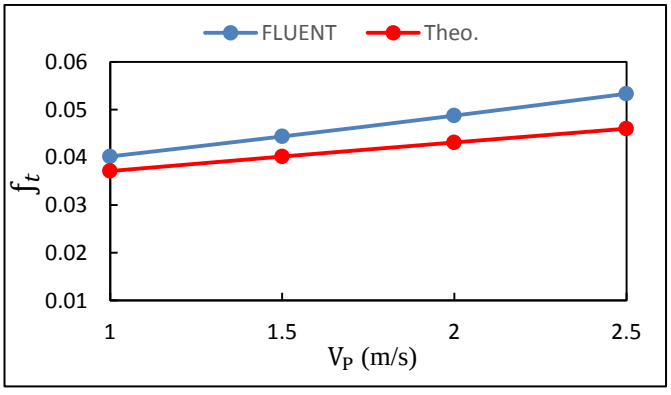

Fig. 32 Variation of friction factor with perforation velocity.

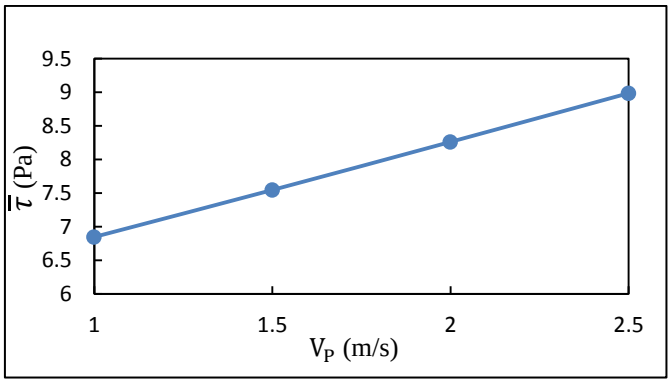

Fig. 33 Variation of average shear stress with perforation velocity.

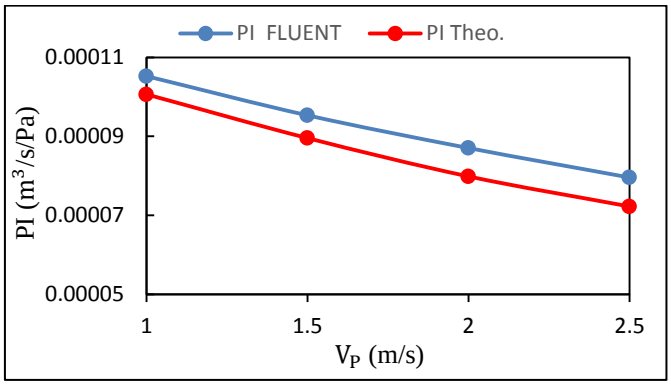

Fig. 34 Variation of productivity index with perforation velocity.

12. Conclusions

The effect of pressure drop, friction factor, shear stress and productivity index on the performance of perforated vertical wellbores was studied. It was simulated by using ANSYS FLUENT numerically, and the results obtained were numerically compared with the theoretical equations. From the results obtained in this study, the following conclusions can be presented:

1. The increase in the density of the perforations for the different phase angle causes an increase in pressure drop, friction factor, and shear stress, but decreases the productivity index.
2. The effect of the phase angles of the perforations is very small on the pressure drop, friction factor, shear stress, and productivity index, so it can be neglected.
3. The effect of friction pressure drop is about 66 % of total pressure drop, while the acceleration pressure drop is approximately 34 % according to the numerical results. According to the theoretical results, the friction pressure drop was about 62 %, the acceleration pressure drop is 29 % and the mixing pressure drop is 7 %.
4. Increase the diameter and velocity of the perforations, lead to increasing the total pressure drop due to the increasing flow rate of crude oil into the wellbore.
5. Comparing the numerical results by using FLUENT with theoretical results by using equations the average error was about 9 %.

References

[1] Metin Karakas and S. M. Tariq, "Semi analytical Productivity Models for Perforated Completions", SPE Production Engineering, Vol. 6, Issue 1, pp. 73-82, February 1991.

[2] Joseph Ansah, Mark A. Pruett and Mohamed Y. Soliman, "Advances in Well Completion Design: A New 3D Finite-Element Wellbore Inflow Model for Optimizing Performance of Perforated Completions", Society of Petroleum Engineers Source, International Symposium and Exhibition on Formation Damage Control, 20-21 February 2002, Lafayette, Louisiana, pp. 1-11, 2002.

[3] Turhan Yildiz, "Productivity of Selectively Perforated Vertical Wells", Society of Petroleum Engineers Source, SPE Journal, Vol. 7, Issue 2, pp. 158-169, June 2002.

[4] Jacques Hagoort, "An analytical model for predicting the productivity of perforated wells", Elsevier, Journal of Petroleum Science and Engineering, Vol. 56, Issue 4, pp. 199-218, 2007.

[5] Zeboudj Faycal Fayal and Bahi Lakhdar, "Horizontal Well Performance Flow Simulation CFD-Application", Society of Petroleum Engineers, SPE Production and Operations Conference and Exhibition, 8-10 June, Tunis, Tunisia, June 2010.

[6] J. Xu, J. Hu, M. Luo, S. Wang, B. Qi and Z. Qiao, "Optimization of Perforation Distribution in HTHP Vertical Wells", The Canadian Journal of Chemical Engineering, Vol. 91, No. 2, December 2011.

[7] Mohammed Abdulwahhab Abdulwahid, Sadoun Fahad Dakhil and I. N. Niranjan Kumar, "Numerical analysis of fluid flow properties in a partially perforated horizontal wellbore", American Journal of Energy Engineering, Vol. 2, No. 6, pp. 133-140, December 2014.

[8] Mahmoud O. Elsharafi and Tibor Bodi, "Evaluation of the productivity of vertical oil wells by using different high shot density (HSD) guns", International Journal of Petrochemical Science & Engineering, Vol. 2, Issue 2, March 2017.

[9] Mohammed K. Salim, Hussein S. Sultan and Ahmed K. M. AL-Shara, "Effect of Shape and Parameters of Perforation in a Vertical Wellbore with Two Perforations (without Porous Media) on Pressure Drop", Fluid Mechanics, Vol. 4, Issue 3, June 2017.

[10] FLUENT Inc., FLUENT 6.3 User's Guide, 2006.

[11] Mohammed Abdulwahhab Abdulwahid, Niranjan Kumar Injeti and Sadoun Fahad Dakhil, "Numerical Simulation of Flow through Wellbore for Horizontal Wells", Proceedings of the 2013 International Conference on Applied Mathematics and Computational Methods in Engineering, pp. 40-48, 2013.

[12] Mohammed Abdulwahhab Abdulwahid, Sadoun Fahad Dakhil and I. N. Niranjan Kumar, "Numerical analysis of fluid flow properties in a partially perforated horizontal wellbore", American Journal of Energy Engineering, Vol. 2, No. 6, pp. 133-140, December 2014.

[13] Thomas Vyzikas, "Application of numerical models and codes", MERiFIC, Marine Energy in Far Peripheral and Island Communities, February 2014.

[14] H. K. Versteeg and W. Malalasekera, "An Introduction to Computational Fluid Dynamics, the Finite Volume Method", 2nd Edition, Prentice Hall, ISBN: 978-0-13-127498-3, 2007.

[15] S. D. Joshi, "Cost/Benefits of Horizontal Wells", Society of Petroleum Engineers, SPE Western Regional/AAPG Pacific Section Joint Meeting, 19-24 May, Long Beach, California, 2003.

[16] F. Moukalled, L. Mangani and M. Darwish, "The Finite Volume Method in Computational Fluid Dynamics", Spniger, ISBN 978-3-319-16874-6, 1st Edition, 2016.

[17] Morris Muskat, "The Effect of Casing Perforations on Well Productivity", Society of Petroleum Engineers, Transactions of the AIME, Vol. 151, Issue 1, pp. 175-187, December 1943.

[18] Ruben M. S. M. Schulkes and Ole Harald Utvik, "Pressure Drop in a Perforated Pipe with Radial Inflow: Single-Phase Flow", Society of Petroleum Engineers, SPE Journal, Vol. 3, Issue 1, pp. 77-85, March 1998.

[19] Li Hua, Lu Yan, Peng Xiaodong, Lv Xindong and Wang Laichao, "Pressure Drop Calculation Models of Wellbore Fluid in Perforated Completion Horizontal Wells", IJHT, International Journal of Heat and Technology, Vol. 34, No. 1, pp. 65-72, March 2016.

[20] S. E. Haaland, "Simple and Explicit Formulas for the Friction Factor in Turbulent Pipe Flow", Journal of Fluids Engineering, Vol. 105, No. 1, pp. 89-90, March 1983.

[21] Harald Asheim, Johnny Kolnes and Piet Oudeman, "A flow resistance correlation for completed wellbore", Journal of Petroleum Science and Engineering, Vol. 8, Issue 2, pp. 97-104, September 1992.

[22] Ze Su and J. S. Gudmundsson, "Pressure Drop in Perforated Pipes: Experiments and Analysis", Society of Petroleum Engineers, SPE Asia Pacific Oil and Gas Conference, 7-10 November, Melbourne, Australia, pp. 563-574, November 1994.

[23] Mohammed K. Salim, Hussein S. Sultan and Ahmed K. M. AL-Shara, "Numerical Simulation of Perforated Vertical Wellbore", M. Sc. Thesis, Mechanical Engineering Department, University of Basrah, April, 2017.

Nomenclature

Symbol	Description	Units
A	Area	m^2
D	Wellbore Diameter	m
d	Perforation Diameter	m
e	Roughness	m
l	Perforation Length	m
Q	Main Flow Rate	m^3/s
q	Inflow Rate from Perforation	m^3/s
ΔP	Pressure Drop	Pa
f	Friction Factor	-
n	Number of perforations	
spm	Shot per meter	

Greek symbols

Symbol	Description	Units
μ	Fluid Viscosity	kg/m.s
ρ	Density	kg/m^3
α	Angle Inflow from Perforation	deg.
Θ	Phase Angle	deg.

Subscripts

Symbol	Description
1	Inlet
2	Perforation
3	Outlet
acc.	Acceleration
f	Friction
g	Gravity
i, j	Vector
m	Main Pipe
o	Unperforated

Appendix 1

Grid No.	Max Size	Total Nodes	Pressure Drop (Pa)	Pressure at Center (Pa)
1	0.009	101635	266.989	135.927
2	0.00875	104679	267.049	135.791
3	0.0085	106201	267.174	135.368
4	0.00825	125109	267.556	137.316
5	0.008	140721	274.029	132.075
6	0.00775	144597	274.112	131.969
7	0.0075	148473	274.181	131.862
8	0.00725	136212	274.163	131.002
9	0.007	179083	274.035	131.554
10	0.00675	183503	274.121	131.421
11	0.0065	190133	274.238	131.205
12	0.00625	213179	274.746	129.592
13	0.006	247065	274.636	128.692
14	0.00575	295294	274.413	128.486
15	0.0055	299337	274.418	128.401
16	0.00525	333889	275.872	127.836
17	0.005	386955	277.792	126.321
18	0.00475	404965	281.075	125.651
19	0.0045	498793	285.119	122.975
20	0.00425	524149	285.267	122.536
21	0.004	645077	287.813	121.097
22	0.00375	743613	287.526	121.099
23	0.0035	901767	290.266	121.028
24	0.00325	1044173	291.534	120.641
25	0.003	1361151	292.343	119.814